

# STOCHASTIC PROCESSES OF SOIL PRODUCTION AND TRANSPORT: EROSION RATES, TOPOGRAPHIC VARIATION AND COSMOGENIC NUCLIDES IN THE OREGON COAST RANGE

ARJUN M. HEIMSATH<sup>1\*</sup>, WILLIAM E. DIETRICH<sup>2</sup>, KUNIHICO NISHIZUMI<sup>3</sup> AND ROBERT C. FINKEL<sup>4</sup>

<sup>1</sup>Department of Earth Sciences, 6105 Fairchild Hall, Dartmouth College, Hanover, NH 03755-3571, USA

<sup>2</sup>Department of Geology and Geophysics, University of California, Berkeley, CA 94720, USA

<sup>3</sup>Space Sciences Laboratory, University of California, Berkeley, CA 94720, USA

<sup>4</sup>Center for Accelerator Mass Spectrometry, Lawrence Livermore National Laboratory, Livermore, CA 94550, USA

Received 17 April 2000; Revised 16 October 2000; Accepted 8 December 2000

## ABSTRACT

Landscapes in areas of active uplift and erosion can only remain soil-mantled if the local production of soil equals or exceeds the local erosion rate. The soil production rate varies with soil depth, hence local variation in soil depth may provide clues about spatial variation in erosion rates. If uplift and the consequent erosion rates are sufficiently uniform in space and time, then there will be tendency toward equilibrium landforms shaped by the erosional processes. Soil mantle thickness would adjust such that soil production matched the erosion. Previous work in the Oregon Coast Range suggested that there may be a tendency locally toward equilibrium between hillslope erosion and sediment yield. Here results from a new methodology based on cosmogenic radionuclide accumulation in bedrock minerals at the base of the soil column are reported. We quantify how soil production varies with soil thickness in the southern Oregon Coast Range and explore further the issue of landscape equilibrium. Apparent soil production is determined to be an inverse exponential function of soil depth, with a maximum inferred production rate of  $268 \text{ m Ma}^{-1}$  occurring under zero soil depth. This rate depends, however, on the degree of weathering of the underlying bedrock. The stochastic and large-scale nature of soil production by biogenic processes leads to large temporal and spatial variations in soil depth; the spatial variation of soil depth neither supports nor rejects equilibrium morphology. Our observed catchment-averaged erosion rate of  $117 \text{ m Ma}^{-1}$  is, however, similar to that estimated for the region by others, and to soil production rates under thin and intermediate soils typical for the steep ridges. We suggest that portions of the Oregon Coast Range may be eroding at roughly the same rate, but that local competition between drainage networks and episodic erosional events leads to landforms that are out of equilibrium locally and have a spatially varying soil mantle. Copyright © 2001 John Wiley & Sons, Ltd.

KEY WORDS: erosion; soil production; landscape evolution; dynamic equilibrium;  $^{10}\text{Be}$  and  $^{26}\text{Al}$

## INTRODUCTION

Hilly and mountainous landscapes around the world are mantled with soil. In regions where external sources of sediment (e.g. aeolian and glacial deposition) are absent or negligible, the soil mantle is typically produced from the underlying bedrock. Gilbert (1877) first suggested that the rate of soil production from the underlying bedrock is a function of the depth of the soil mantle. We term this rate law the soil production function (Heimsath *et al.*, 1997), defined as the relationship between soil depth and the rate of bedrock conversion to soil. The soil depth that sets the rate of soil production is a result of the balance between the soil production and erosion. If local soil depth is constant over time, the soil production rate equals the erosion rate, which equals the lowering rate of the land surface. Understanding the evolution rates of soil-mantled landscapes is furthered therefore by quantifying the soil production function (Anderson and Humphrey, 1989; Rosenbloom and Anderson, 1994; Dietrich *et al.*, 1995; Heimsath *et al.*, 1997). Heimsath *et al.* (1997, 1999, 2000) reported spatial variation of erosion rates, suggesting that the landscapes were out of the state of

\* Correspondence to: A. M. Heimsath, Department of Earth Sciences, 6105 Fairchild Hall, Dartmouth College, Hanover, NH 03755-3571, USA. E-mail: arjun.heimsath@dartmouth.edu

Contract/grant sponsor: NSF; contract/grant number: EAR-9527006.

Contract/grant sponsor: Cal Space; contract/grant number: IGPP-LLNL G596-05.

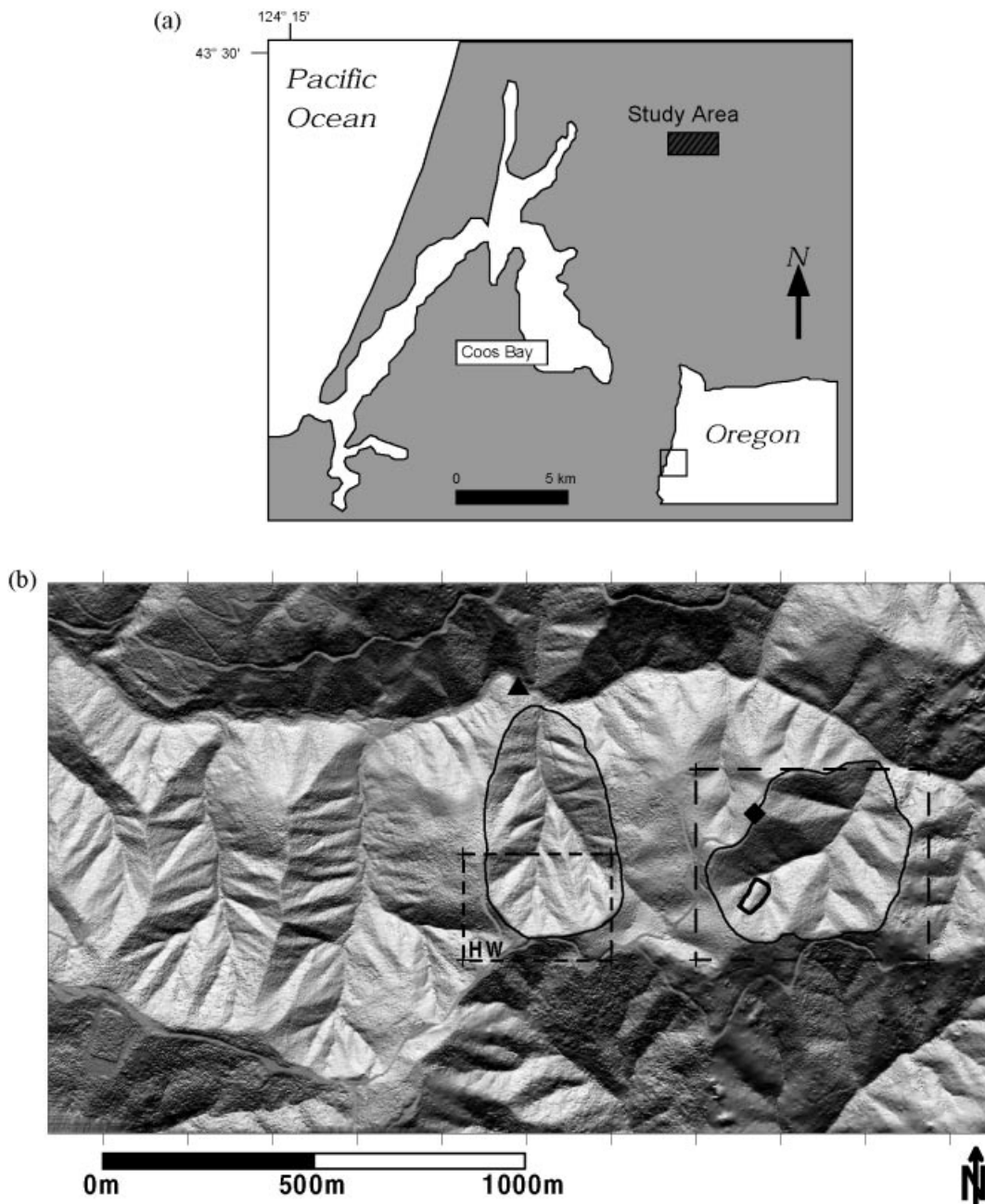


Figure 1. (a) Site map showing the Coos Bay region as outlined by the rectangle on the state map of Oregon. The shaded region labelled 'Study Area' is the field area shown in (b). (b) Shaded relief map of the field area in the Oregon Coast Range generated from laser altimetry elevation data. The two outlines represent a larger area of the landscape similar in morphology to the noses studied in the Headwall (HW) region and on the nose, Coos3, which are shown in detail for the area within the dashed lines in Figure 4a and b, respectively. The black triangle near the outlet of the HW catchment shows the location of the stream sediment samples, OR-16 and 17, from Sullivan Creek. The black diamond on the edge of the eastern subcatchment shows the location of OR-26, the only nuclide sample not in the HW study area. Adapted from Roering *et al.* (1999). (c) Oblique aerial photograph showing clear-cut slopes of the field area, looking due west such that the basin in the lower right corner corresponds to the second basin from the left edge of (b). Note the steep slopes, the ridge and valley topography, and the consistency of elevation on the main ridge crest



Figure 1. Continued

dynamic equilibrium, as first conceptualized by Gilbert (1877, 1909) and then Hack (1960), where the landscape morphology is time-independent.

On actively eroding hilly landscapes, characterized by ridge and valley topography, the colluvial soil mantle is typically thin and is produced and transported by mechanical processes. Tree-throw, animal burrowing and similar processes, such as freeze–thaw and shrink–swell cycles, convert in-place bedrock to a mobile, often rocky, soil layer that is then transported downslope by the same actions (Lutz and Griswold, 1939; Lutz, 1960; Hole, 1981; Mitchell, 1988; Matsuoka, 1990; Schaetzl and Follmer, 1990; Norman *et al.*, 1995; Paton *et al.*, 1995). On steep slopes, shallow landsliding also transports material downslope, and may play a role in producing soil. While such processes are aided directly, and even accelerated, by chemical weathering of the bedrock, they are able to produce soil from bedrock irrespective of its weathered state. Previous quantification of the soil production function focused on low gradient topography developed on relatively homogenous bedrock, where the geomorphic processes could be characterized by simple rate laws (Heimsath *et al.*, 1997, 1999, 2000).

In this paper we examine the steep, soil-mantled landscape of the Oregon Coast Range where we observed that stochastic processes of tree-throw and shallow landsliding may dominate soil production and transport. We apply the methods of Heimsath *et al.* (1999) to determine apparent soil production rates under such conditions, and specifically address the potential effects of these processes on our methods of using *in situ*-produced cosmogenic nuclide concentrations as well as the landscape morphology to determine soil production rates. This paper also seeks to understand the competition between the spatial variation of processes and topography, which suggests large variations in local erosion rates, and the potential for dynamic equilibrium for the region, forwarded by Reneau and Dietrich (1991), who found hillslope erosion and sediment yield to be in an approximate balance over a range of spatial and temporal scales.

#### FIELD SITE

The study area shown in Figure 1 is an intensely studied, humid-temperate, soil-mantled and hilly landscape. Extensive research was conducted in the region to understand the hydrologic and geomorphic processes

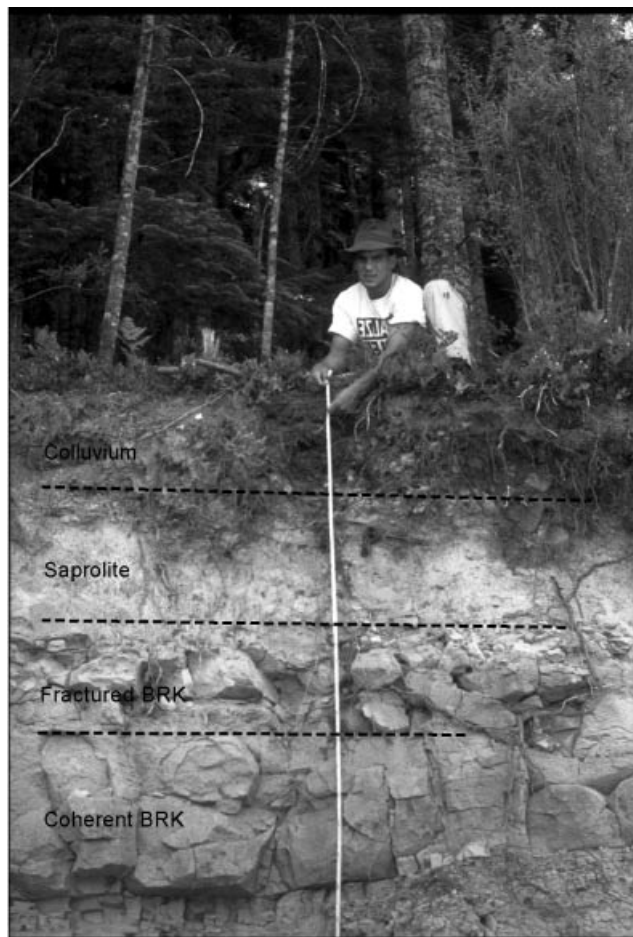


Figure 2. Photograph of a cross-section shown in a road cut in the study area. The material labelled and roughly delineated with dashed lines is typical of the Oregon Coast Range soil to bedrock profiles. Note that the coherent bedrock in this profile is similar to the bedrock exposed on strongly divergent ridge crests

operating on the hillslopes (e.g. Dietrich and Dunne, 1978; Dietrich *et al.*, 1986; Reneau and Dietrich, 1990, 1991; Montgomery *et al.*, 1997; Roering *et al.*, 1999). The bedrock underlying the region is a relatively undeformed, thick sequence of arkosic and lithic Eocene turbidite sandstone and siltstone called the Tye Formation (also called the Flourney Formation) (Snively *et al.*, 1964; Lovell, 1969; Heller *et al.*, 1985). Bedrock outcrops on some of the steeper ridge crests and in the first-order tributaries are coherent and relatively unweathered. Bedrock exposed by numerous road cuts along the ridges is extensively weathered and fractured, often as a saprolite that has developed in places for several metres (Figure 2). Anderson (1995) showed that while the bedrock can be weathered and mechanically weak, the weathered condition may be associated with relatively minor chemical alteration. The study site is typical of the Oregon Coast Range, where the steep landscape was densely forested with Douglas fir, other large conifers and mixed hardwoods. Parts of the study area and the adjacent hillslopes were clear-cut in 1987 and replanted exclusively with Douglas fir in 1989.

Rainfall in the region falls primarily over the winter months and averages about 200 cm a<sup>-1</sup> (Haagen, 1989). The site elevation is about 300 m along the first major ridgeline inland from the Pacific Ocean. While the region is directly above the Cascadia subduction zone, the uplift rates have been variable both in the

Quaternary (West and McCrumb, 1988; Kelsey, 1990; Kelsey and Bockheim, 1994) and over the last 20–30 Ma (Orr *et al.*, 1992). Rock uplift rates are estimated between 30 and 230 m Ma<sup>-1</sup> by dating marine terraces in the central Coast Range, just north of the study area (Kelsey and Bockheim, 1994; Kelsey *et al.*, 1994). Personius (1995) estimated similar rates of 100–300 m Ma<sup>-1</sup> for the central Coast Range (also north of the study area) by dating strath terraces along many of the rivers draining the Coast Range. There have been studies measuring sediment yield from Oregon Coast Range streams (e.g. Brown and Krygier, 1971; Beschta, 1978), but the data could reflect contemporary land-use patterns of the area. Despite this concern, such sediment yield studies estimating basin-wide denudation rates of 50–80 m Ma<sup>-1</sup> agree roughly with the average bedrock lowering rates of 70 m Ma<sup>-1</sup> determined by Reneau and Dietrich (1991) for undisturbed basins, leading to their suggestion that the landscape is in approximate large-scale equilibrium.

The convex-up ridges are thinly mantled (0–1.5 m) with an organic-rich, colluvial soil. The low density (0.8–1.2 g cm<sup>-3</sup>), silt-sand soil matrix supports rock clasts derived from the underlying bedrock, or transported from upslope. Thinner soils (<50 cm) are generally on the side slopes and the narrower noses; they are rocky, and can be hard to distinguish from the underlying fractured bedrock. The fractured bedrock retains some of the rock structure of the massive sandstone, while the colluvial rocks are haphazardly distributed. Deeper soils tend to have a much lower proportion of colluvial rocks at depth and typically mantle a mechanically weak saprolite. Saprolite retains the relic rock structure of the sandstone yet is significantly more susceptible to mechanical weathering (it was easily penetrated by a hand auger or rock hammer). The soil–bedrock boundary on the saprolite is distinguishable by the change in colour from dark brown soil to light tan, orange saprolite, and by the change in texture to the more sandy saprolite with little to no organic content.

The appearance and spatial variation of the weathered profile in the study can be divided into five layers: (1) soil, (2) saprolite, (3) pervasively oxidized but competent rock, (4) fractured, partially oxidized rock and (5) unweathered sandstone (Figure 2) (Anderson, 1995). Massive, relatively unweathered sandstone is common at the base of hollows evacuated by recent debris flows and along some of the more sharply convex ridge crests. The spatial distribution of the coherent, unweathered bedrock appears to play a role in determining the soil production and transport processes as neither tree roots nor burrowing mammals can easily penetrate it as readily as they can the saprolite.

## SOIL PRODUCTION AND TRANSPORT

Soil appears to be produced primarily by the mechanical disruption of the underlying bedrock caused by root penetration and burrowing animals. While the roots of virtually all species of vegetation were observed to penetrate the fractured bedrock beneath thin soils (Schmidt, 1999), the impact of a mature Douglas fir tree falling over is likely to be the most significant soil-producing mechanism. Mature trees can have root-wads that are on the order of 3–5 m in diameter and the pits left when such trees fall can be greater than 1 m deep (examples from other field areas: Stephens, 1956; Denny and Goodlett, 1957; Lyford and MacLean, 1966; Schaetzel and Follmer, 1990; Norman *et al.*, 1995). If, for an example from the upper end of field observations, a tree-fall creates a 5 m diameter pit that extends 50 cm into the underlying bedrock, the effective lowering of that part of the landscape is 50 cm. To put the effect of such a process into context, note that the average bedrock lowering rate calculated by Reneau and Dietrich (1991) was 70 m Ma<sup>-1</sup>, which suggests that 0.5 m of vertical lowering caused by a single tree-fall accounts for about 7000 years of local soil production.

Sediment transport by tree-throw is an important factor as well (e.g. Lutz and Griswold, 1939; Lyford and MacLean, 1966; Dietrich *et al.*, 1982; Paton *et al.*, 1995). When a tree falls it creates a pit and not all of the uprooted sediment moves downhill: some may return to the pit and some will spread to the sides. Norman *et al.* (1995) report detailed findings on pit and mound volumes as functions of topographic slope and found that on progressively steeper slopes tree-throw became an increasingly important component of mass wasting. They found that for tree-throw mounds above 47° slopes almost all the uprooted sediment is transported downslope rather than returning to the pit. Additionally, the pit resulting from tree-throw creates a significant change in local slope, disrupting the continuity of sediment transport from uphill, and creating a sink for

sediment. The tendency is for tree-throw pits to fill relatively rapidly with soil from the surrounding slopes such that the hillslope returns to its pre-tree-throw form (e.g. Lutz, 1940; Stephens, 1956; Schaetzl and Follmer, 1990). Estimates based on the Schaetzl and Follmer (1990) study and those of Stephens (1956), Lutz (1960), Lyford and MacLean (1966) and Norman *et al.* (1995) suggest that tree fall densities may have been about 15–20 per cent of the area prior to logging. The result is that soil depth can be extremely variable depending on the stochastic nature of tree-throw.

Tree-throw is not the only cause of soil production and transport on the hillslopes of the field area. Mountain beaver (*Aplodontia rufa*) colonies are prevalent except on the sharply convex ridge crests where bedrock outcrops. Their burrows can be as wide as 50 cm and are commonly observed near fallen trees. While their burrowing tends to be in soil, evidence of burrowing was observed in the saprolite and fractured bedrock exposed in soil pits. Piles of fresh material outside their burrows typically contained fractured sandstone clasts, although these could also be the colluvial stones from the soil column. The high density of mountain beavers in the field area, and the ease with which the fractured bedrock and saprolite could be mobilized into the soil column suggests that their role in soil production is significant. They are certainly primary transporters of soil as their burrowing is a continuous process while they search for fresh roots to chew on for their source of moisture and food intake (e.g. Beier, 1989; Bleich and Racine, 1991; Fitts, 1996).

Shallow landsliding and debris flows also play important roles in transporting sediment off the steeper slopes of the Oregon Coast Range and out of the colluvial hollows (e.g. Pierson, 1977; Yee and Harr, 1977; Dietrich and Dunne, 1978; Dietrich *et al.*, 1986; Johnson and Sitar, 1990; Benda and Dunne, 1997). Debris flows may be the primary mechanism for sediment removal from the steep headwater catchments and they can commonly excavate the first-order colluvial-filled hollows and transport the sediment well into the third-order catchments. While shallow landsliding does occur on the steep, planar slopes found near the base of the hillslopes, it is a rare process on or near the convex ridge crests. Importantly, shallow landsliding and debris flows commonly expose the underlying bedrock and make it more susceptible to ravelling, wetting–drying, and freeze–thaw processes.

### CONCEPTUAL FRAMEWORK

Field observations of the biogenic activity in the Oregon Coast Range suggested that the dominant soil production processes act perpendicular to the ground surface. Tree roots grow parallel to the surface and the mountain beavers appear to burrow approximately normal to the surface (observed where slopes are relatively steep). It may also be likely that smaller biota, such as gophers, earthworms and understorey vegetation, favour the shortest distance between the ground surface and the soil–bedrock boundary, which is the slope-normal depth,  $H$  (Figure 3). Previously, the theoretical framework of Dietrich *et al.* (1995) was developed by Heimsath *et al.* (1997, 1999) to examine the relationship between soil production, topographic curvature and soil thickness (see also Kirkby, 1967; Kirkby, 1971; Ahnert, 1987; Anderson and Humphrey, 1989). The continuity equation for a vertical column of soil,  $h$ , neglecting mass loss to solution, was written as:

$$\rho_s \frac{\partial h}{\partial t} = -\rho_r \frac{\partial z_b}{\partial t} - \nabla \cdot \tilde{q}_s \quad (1)$$

where the vertical lowering rate of the soil–bedrock boundary,  $-\partial z_b/\partial t$ , at any point on the landscape is equivalent to the slope-normal soil production rate,  $\varepsilon(H)$ , observed here, multiplied by the secant of the slope angle,  $\theta$  (for moderate slopes  $\sec(\theta) \sim 1$ ) (Heimsath *et al.*, 2000). Bulk densities of soil and rock, respectively, are  $\rho_s$  and  $\rho_r$ . Early work, proposed by Davis (1892) and Gilbert (1909) and then initially modelled by Culling (1960, 1963), Kirkby (1967) and Hirano (1968) and many others subsequently, suggested that convex landforms were formed by sediment transport processes where the mass flux is linearly proportional to slope:

$$\tilde{q}_s = -\rho_s K \nabla z \quad (2)$$

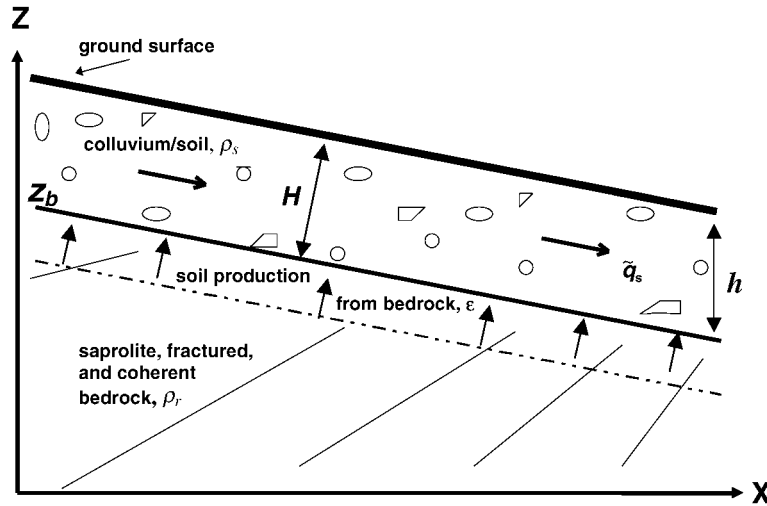


Figure 3. The conceptual framework as used by Heimsath *et al.* (1997) for vertical soil depth,  $h$ , showing how the slope-normal depth,  $H$ , is equal to the vertical depth multiplied by the secant of the slope angle. The change in soil mass in a column of soil with time is equal to the vertical production of soil from the underlying bedrock minus the divergence of sediment transport. Note that  $z = e + H \sec\theta$  and that the vertical lowering rate of the soil–bedrock interface is equal to the normal soil production multiplied by the secant of the slope angle. This is a bedrock-fixed coordinate system with  $h \ll$  the scale of landscape elevation set by the total relief

where  $K$  is analogous to a diffusion coefficient with dimensions  $L^2T^{-1}$ , and  $z$  is the ground surface elevation. If local steady-state conditions apply, that is assuming that soil thickness at any point is constant (i.e.  $\partial h / \partial t = 0$ ), then Equation 1 reduces to a simple relationship between vertical soil production and the divergence of sediment transport:

$$-\rho_r \frac{\partial z_b}{\partial t} = -\nabla \cdot \tilde{q}_s \tag{3}$$

When the linear sediment transport law (Equation 2) is substituted into Equation 3, the familiar relationship between soil production (or, more commonly, erosion) and topographic curvature is obtained:

$$-\frac{\partial z_b}{\partial t} = -\frac{\rho_s}{\rho_r} K \nabla^2 z \tag{4}$$

Heimsath *et al.* (1997, 1999, 2000) used measurements of soil depth and topographic curvature to report that curvature (a proxy for soil production by Equation 4) declined with increasing soil thickness, thus empirically defining the form of the soil production function. Field measurements of curvature and depth were complemented with soil production rates determined from *in situ*-produced cosmogenic nuclides (described below) such that the soil production rates,  $\varepsilon(H)$ , were found to be well defined inverse exponential functions of soil depth,

$$-\frac{\partial z_b}{\partial t} = \varepsilon(H) \sec\theta = \varepsilon_0 e^{-\alpha H} \tag{5}$$

where  $\varepsilon_0$  is the soil production rate under zero soil depth. Substituting Equation 5 in Equation 4 suggests that

there should be an exponential relationship between curvature and soil depth:

$$-\nabla^2 z = \frac{\varepsilon_0 \rho_r}{K \rho_s} e^{-\alpha H} \quad (6)$$

which was supported by the data of Heimsath *et al.* (1997, 1999). Heimsath *et al.* (2000) report a clear linear relationship between curvature and depth from a different field area, suggesting that a simple diffusive transport law is not always adequate.

While there was some field support for the linear transport law on low to moderate gradients (Schumm, 1967; McKean *et al.*, 1993), recent studies (e.g. Kirkby, 1985; Anderson, 1994; Howard, 1994, 1997; Roering *et al.*, 1999) suggested that sediment transport depends non-linearly on slope, especially on steeper gradients, such that Roering *et al.* (1999) write:

$$\tilde{q}_s = \frac{K_{nl} \nabla z}{1 - \left( \frac{|\nabla z|}{S_c} \right)^2} \quad (7)$$

where  $S_c$  is the critical hillslope gradient and the non-linear diffusivity,  $K_{nl}$ , is not necessarily the same as  $K$ . Substituting Equation 7 in Equation 3 for steady-state conditions leads to:

$$E = -\frac{K_{nl}}{\frac{\rho_r}{\rho_s}} \left[ \frac{\nabla^2 z}{1 - \left( \frac{|\nabla z|}{S_c} \right)^2} + \frac{2(z_x^2 z_{xx} + z_y^2 z_{yy} + 2z_x z_y z_{xy})}{S_c^2 \left( 1 - \left( \frac{|\nabla z|}{S_c} \right)^2 \right)^2} \right] \quad (8)$$

where  $E = -\partial z_b / \partial t$ , and suggests that local erosion rates for the non-linear sediment transport equation can be calculated using topographic derivatives alone with estimates of  $K_{nl}$  and  $S_c$ . Roering *et al.* (1999) assume equilibrium conditions for the landscape, such that every point is lowering at the same rate,  $C_0$ , to calibrate their model and deduce optimal values for  $K_{nl}$  and  $S_c$ .

To evaluate the implications of this conceptual framework for a landscape that might be in dynamic equilibrium, the hypothetical equilibrium lowering rate ( $\text{m Ma}^{-1}$ ) is defined as:

$$C_0 = -\frac{\partial z}{\partial t} \quad (9)$$

which equals Equation 4 or 5 if local soil depth is constant over time, such that:

$$E_0 e^{-\alpha H} = C_0 \cos(\theta) \quad (10)$$

Solving Equation 10 yields the following expression for the equilibrium normal soil depth as a function of the natural log of the slope angle,  $\theta$ :

$$H = -\frac{1}{\alpha} \ln \left( \frac{C_0}{\varepsilon_0} \cos \theta \right) \quad (11)$$

Equation 11 states simply the expected relationship between normal soil depth and slope given that the vertical lowering rate,  $C_0$ , must be the same everywhere on the landscape. That is, thinner normal soil depths on steeper slopes driving higher surface-normal soil production.

These analytical expressions thus define a field-testable series of hypotheses that will help determine the soil production function as well as provide a test for landscape equilibrium. Namely, high-resolution measurements of soil depth and the land surface elevation will define the form of either Equations 6 and 8 (by plotting soil depth against topographic derivatives) or Equation 11 (plotting depth against slope).

### *Cosmogenic nuclides*

The above conceptual framework can lead to the form of the soil production function, but cannot lead to determining the rates of landscape evolution without an independently determined value for  $K$ , or values for  $K_{nl}$  and  $S_c$ . Here we use concentrations of the cosmogenic nuclides,  $^{10}\text{Be}$  and  $^{26}\text{Al}$ , produced *in situ* in bedrock, saprolite and quartz grains extracted from sediments to determine rates of erosion (see reviews in Lal, 1991; Nishiizumi *et al.*, 1993; Bierman, 1994; Cerling and Craig, 1994) and soil production (Heimsath *et al.*, 1997, 1999). Nuclide concentrations measured from quartz are dependent on the production and decay rates of the nuclide, as well as the erosion rate of the sample, such that they reflect the exposure history of the sample (Lal and Arnold, 1985; Lal, 1988; Nishiizumi *et al.*, 1986, 1991). As shown by Lal (1991), and neglecting production due to muons, the nuclide concentration,  $C$ , depends on the production of the nuclide as an exponential depth function of the surface production rate,  $P_0$ , and its disintegration constant,  $\lambda$ :

$$\frac{dC}{dt} = P_0 e^{-\mu z_x} - \lambda C \quad (12)$$

where  $z_x$  is mass depth below the ground surface,  $\mu$  is the absorption coefficient (equal to material density divided by the mean attenuation length for cosmic rays,  $\Lambda$ , where  $\Lambda \approx 165 \text{ g cm}^{-2}$ ), and  $\lambda = \ln 2/t_{1/2}$ , where  $t_{1/2} = 1.5 \times 10^6 \text{ a}$  for  $^{10}\text{Be}$  and  $t_{1/2} = 7.01 \times 10^5 \text{ a}$  for  $^{26}\text{Al}$ . Values of  $P_0$  for  $^{10}\text{Be}$  and  $^{26}\text{Al}$  are 6 and 36.8 atoms  $\text{g}^{-1} \text{ a}^{-1}$  at sea level, respectively (Nishiizumi *et al.*, 1989), corrected for latitude and altitude (Lal, 1991). If erosion,  $\varepsilon$ , of the target material is assumed to be constant over the exposure history of the sample, Equation 12 can be solved analytically, such that at secular equilibrium, when  $t \gg (\lambda + \mu\varepsilon)^{-1}$  we get (Lal, 1991):

$$C = C_0 e^{-\lambda t} + P(H, \theta) \left( \frac{1}{\lambda + \mu\varepsilon} \right) \quad (13)$$

where  $P(H, \theta)$  is the nuclide production rate (atom  $\text{g}^{-1} \text{ a}^{-1}$ ) at the soil–bedrock boundary under slope-normal soil depth,  $H$ , on a landsurface with local slope,  $\theta$ , and  $C_0$  is the initial concentration of the nuclide.  $P(H, \theta)$  is calculated as a factor of the surface nuclide production rates (Dunne *et al.*, 1999). When the initial nuclide concentration is assumed to be zero, as is commonly the case for exposure histories of rock emerging under continuous processes of erosion, Equation 13 can be simplified and solved for the erosion or soil production rate;

$$\varepsilon = \frac{1}{\mu} \left[ \frac{P(H, \theta)}{C} - \lambda \right] \quad (14)$$

Under steady-state conditions, erosion equals the vertical rate of lowering of the soil–saprolite interface,  $-\partial z_b / \partial t$ , which equals the slope-normal soil production rate,  $\varepsilon(H)$ , multiplied by the secant of the slope angle.

## METHODS

### *Soil production from morphometry*

To test the relationship between soil depth and slope curvature (a proxy for soil production by Equation 4), we surveyed two different areas (Figure 4) at a high resolution ( $\sim 3 \text{ m}$ ) and used the methods described in Heimsath *et al.* (1999) to calculate topographic curvature by gridding the digital elevation data (by *Kriging*

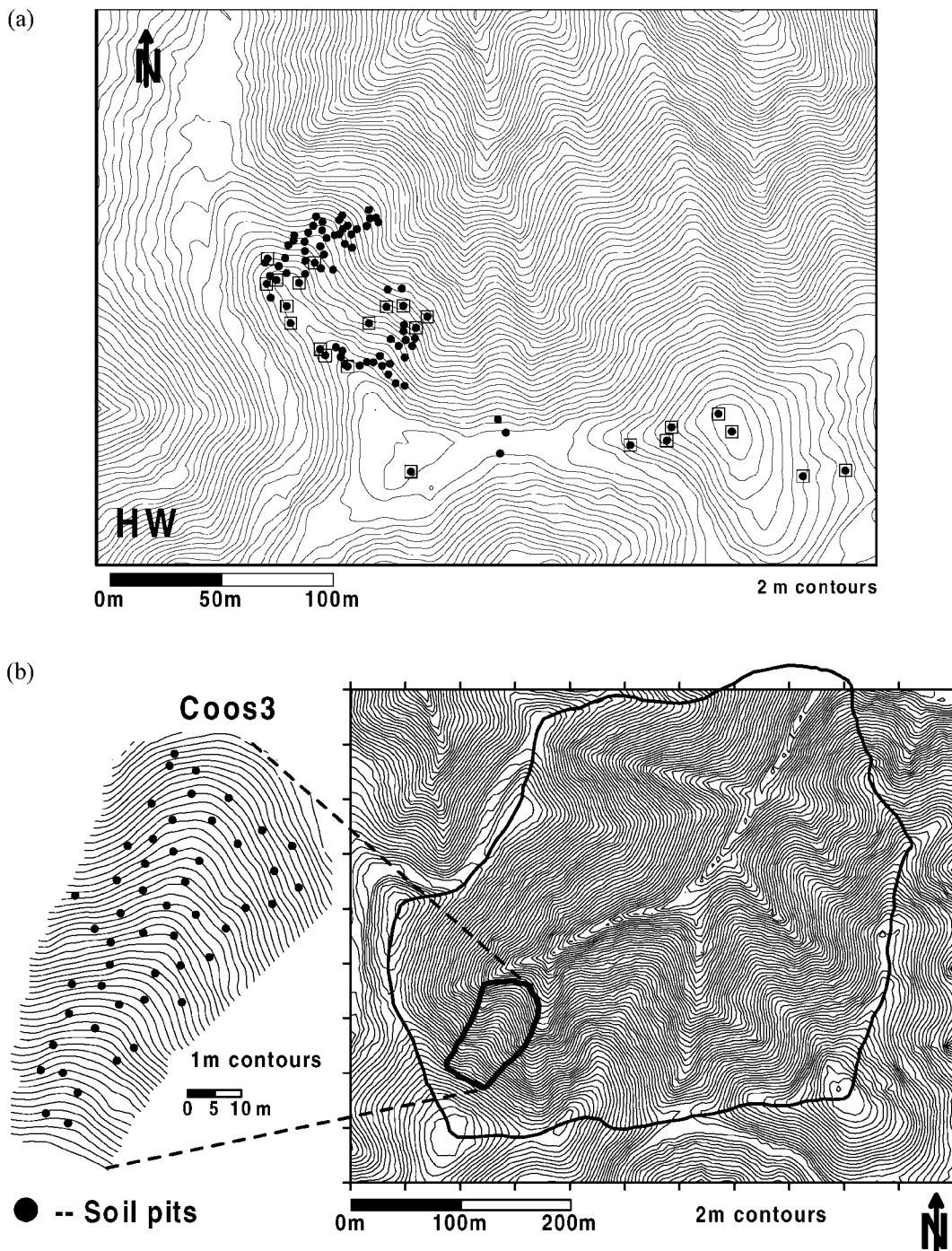


Figure 4. Close-up topographic maps from the same digital elevation data that generated Figure 1b. Contour intervals are 2 m for the area maps and downhill is toward the top of the figures (north). (a) Soil pit locations for the study area in the Headwall (HW) region outlined by the dashed lines in Figure 1b. Soil depth was measured normal to the ground surface in all the pits where the soil–bedrock boundary was clearly defined and continuous over the scale of the pit. A selection of these pits were used to sample the underlying bedrock for the nuclide analyses, indicated by the open squares around the black dots. (b) Soil pit locations and topographic close-up of the Coos3 nose, outlined by the eastern dashed line rectangle on Figure 1b. Contour intervals on the inset map are 1 m. Soil pit locations on both (a) and (b) as well as the topography for Coos3 were surveyed using a total laser survey station

Table I. Soil production rates from cosmogenic nuclide concentrations

Sample	Depth (cm)	Slope	H-slope factor*	Elev. (m)	Wt (g)	Be (mg)	Al (mg)	<sup>10</sup> Be (+/-) (Atoms g <sup>-1</sup> quartz (sea level))	<sup>26</sup> Al (+/-) (sea level)	<sup>26</sup> Al/ <sup>10</sup> Be	+/-	E (m Ma <sup>-1</sup> )	+/-
OR-5	15	39	0.78	246	41.69	0.45	0.10	68586	4243	221468	54774	130.09	34.13
OR-5R	15	39	0.78	246	7.32	1.23	1.23	206870	37634	3060164	174285	174.15	33.61
OR-6	87.5	20	0.32	284	42.89	0.45	9.35	52285	3758	219734	40707	14.70	1.81
OR-7	0	0	1	283	41.85	0.45	10.01	88910	6908	392570	76290	135.19	18.65
OR-7R	0	0	1	283	7.00	1.52	1.52	392570	76290	257021	57911	169.01	32.92
OR-8	42	40	0.465	242	41.54	0.46	1.85	43095	3838	180415	30123	68.56	7.32
OR-8R	42	40	0.465	242	7.29	0.60	10.68	52155	5196	2233161	170271	91.07	18.91
OR-9	0	39	0.94	246	40.19	0.60	9.98	443385	28434	881183	109340	138.73	34.64
OR-10	25	17	0.89	268	40.39	0.60	9.98	209292	21077	989972	110162	203.51	41.47
OR-11	100	20	0.275	290	40.35	0.60	9.43	189720	22007	705523	108864	14.80	2.27
OR-12	95	30	0.25	249	40.18	0.60	9.20	114452	8290	576893	60555	44.06	9.66
OR-15	92	44	0.165	256	40.19	0.61	13.37	60858	5189	297533	44801	26.59	6.01
stream A	145	0	1	190	40.03	0.60	8.28	33990	3257	211864	24860	118.73	39.21
stream B	145	0	1	190	40.18	0.60	9.12	1041276	111508	333345	45848	114.80	34.58
stream B-R	145	0	1	190	40.18	0.60	9.12	189720	22007	976603	143290	116.80	13.39
OR-18	95	41	0.175	254	40.23	0.60	10.80	164825	12032	705523	108864	33.82	7.39
OR-19	75	23	0.35	291	40.36	0.60	12.22	114452	8290	576893	60555	44.75	8.77
OR-21	82	5	0.46	301	40.09	0.45	14.33	107241	8745	494479	96421	37.61	5.49
OR-22	60	30	0.42	249	40.14	0.45	10.42	60858	5189	297533	44801	56.88	8.71
OR-23	60	41	0.34	254	41.52	0.45	11.78	58070	5318	333345	45848	64.13	14.62
OR-24	35	23	0.63	291	40.19	0.45	10.85	40134	2695	256768	30754	113.23	21.15
OR-25	25	22	0.76	285	51.50	0.45	12.79	41472	3054	223654	24426	177.92	29.00
OR-26	58	0	0.54	265	40.29	0.38	9.53	35445	3417	152688	47205	34.39	4.73
OR-27	43	32	0.52	261	40.43	0.45	11.08	58070	5318	333345	45848	106.16	19.22
OR-29	0	12	0.98	271	40.27	0.38	6.00	40134	2695	256768	30754	146.67	22.09
OR-30	10	12	0.92	269	40.25	0.38	5.13	41472	3054	223654	24426	154.87	22.48
OR-31	12	12	0.915	263	36.18	0.38	1.20	42242	4071	113860	33611	169.30	20.42
OR-31R	12	12	0.915	263	7.15	0.38	8.37	42242	4071	113860	33611	239.20	75.39
OR-32	25	15	0.79	263	40.17	0.38	8.37	56232	4172	194075	25968	321.05	102.08
OR-32R	25	15	0.79	263	7.14	0.38	1.72	56232	4172	194075	25968	359.04	122.71
OR-33	30	15	0.76	265	40.63	0.38	6.79	135025	5676	543646	44025	187.26	31.34
OR-33R	30	15	0.76	265	7.58	1.38	1.38	135025	5676	543646	44025	216.08	43.91
OR-34	35	20	0.76	301	41.00	0.38	4.80	135025	5676	543646	44025	69.15	7.87
OR-34R	35	20	0.76	301	7.30	1.28	1.28	135025	5676	543646	44025	68.82	8.40

Concentration errors include  $1\sigma$  from AMS, and all errors are propagated to **E**.

Average soil density:  $1.4 \text{ g cm}^{-3}$ . Depth column is height (cm) above ground for the tor samples

Location: 42.47 N Lat., 124.13 W Long.

<sup>26</sup>Al and <sup>10</sup>Be concentrations from sea level production rates of 36.8 and 6 atoms  $\text{g}^{-1} \text{ a}^{-1}$  (Lal, 1991; Nishizumi *et al.*, 1989)  
\* H-slope factor corrects for soil depth and slope shielding for all samples (Dunne *et al.*, 1999)

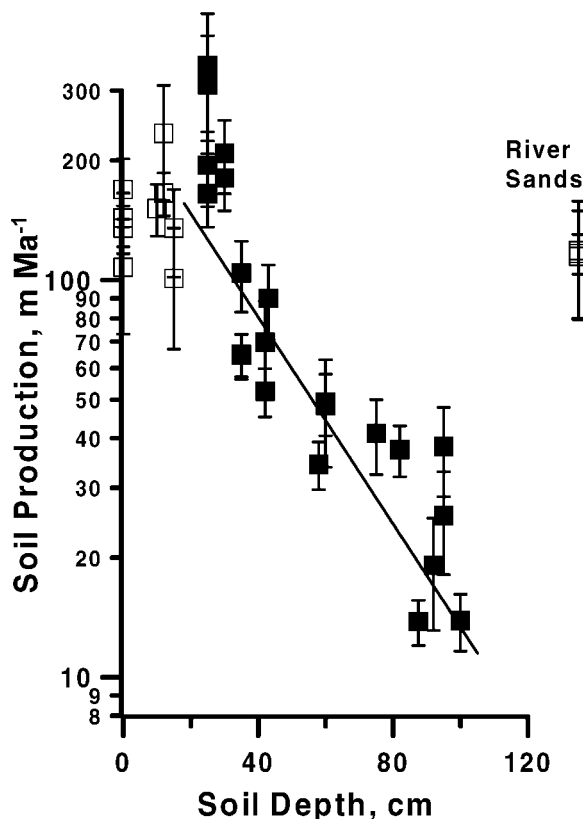


Figure 5. Apparent soil production rates ( $\text{m Ma}^{-1}$ ) calculated from the *in situ*-produced radionuclides,  $^{10}\text{Be}$  and  $^{26}\text{Al}$ , extracted from bedrock samples versus the observed normal soil depth,  $H$ , in cm. The soil production function (Equation 15) is the variance-weighted least-squares fit to the soil production rates under soil depths greater than 15 cm (black squares). Soil production rates for the shallower samples and the exposed bedrock samples (open squares) were not used to determine this function, as discussed in the text. The average erosion rates for the catchment from nuclide concentrations in stream sediments are plotted with open squares to the right of the soil depth axis. All rates are calculated from the concentrations of both nuclides with a few exceptions (Table I). Error bars are  $1\sigma$  propagated from Accelerator Mass Spectrometry (AMS); Atomic Absorption (AA), bulk density, absorption mean free path and soil depth uncertainties

(Cressie, 1991) using *Surfer*<sup>®</sup> software) and using the eight nearest elevation values. We measured soil depth normal to the ground surface in 150 soil pits dug past the soil–saprolite interface. Curvature, the non-linear erosion rates from Equation 8 using Roering *et al.*'s (1999) calibrated values for  $K$  ( $0.0032 \text{ m}^2 \text{ a}^{-1}$ ) and  $S_c$  (1.25), and slopes are plotted against soil depths measured at each soil pit to evaluate the hypotheses outlined above.

#### Cosmogenic nuclides

Soil pits across the full range of observed soil thickness on the divergent noses were used to collect samples from the soil–saprolite boundary, and each sample was taken from the top 5 cm of the continuous layer of saprolite. We selected pits used to collect nuclide samples carefully to avoid any observable effects of recent processes of tree-throw or shallow landsliding. Bulk densities of the saprolite and the overlying soil at selected sites were measured with a cylindrical corer of known volume. Soil thickness was relatively constant within each pit and was measured normal to the slope. Samples of channel sand were collected from Sullivan Creek, immediately downstream of the study area (sample location shown on Figure 1b), to estimate the catchment-averaged erosion rate for the region.

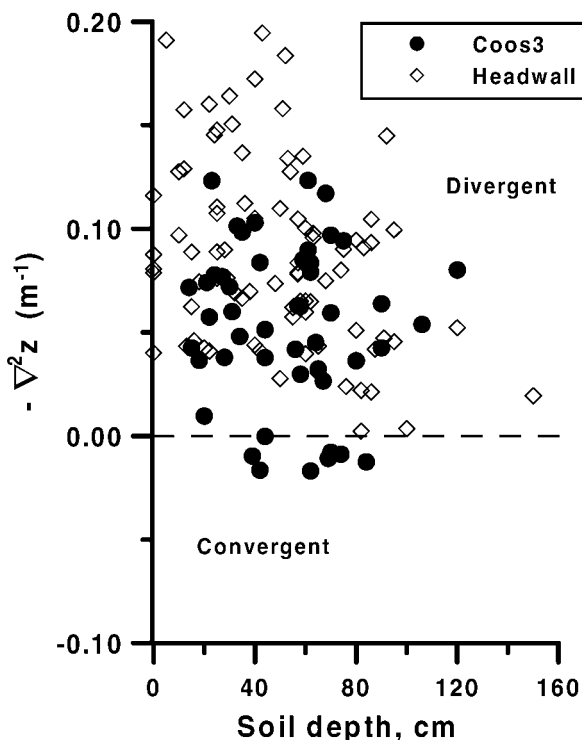


Figure 6. Negative topographic curvature,  $-\nabla^2z$  ( $\text{m}^{-1}$ ), plotted against normal soil depth,  $H$ , measured in the pits shown on Figure 4a and b. Open diamonds are from pits shown in Figure 4a, the Headwall area, and the black dots are from the pits shown in Figure 4b, the Coos3 nose. We calculated curvature with the methodology described in Heimsath *et al.* (1999) using a 5 m grid scale

About 500 g of bedrock, saprolite or sediment from each sample were crushed, sieved to separate particles less than 1 mm size, and chemically purified following the procedure of Kohl and Nishiizumi (1992) to yield about 40 g of quartz from which Be and Al were extracted. Additional samples were collected and processed for  $^{26}\text{Al}$  analyses alone from seven pits as duplicates. We spiked the samples for  $^{10}\text{Be}$  measurement with a  $^9\text{Be}$  carrier solution calibrated by Nishiizumi's Be atomic absorption standard that differed by less than 2 per cent from the Be carrier used for the Nishiizumi *et al.* (1989) analyses. We measured concentrations of  $^{10}\text{Be}$  and  $^{26}\text{Al}$  at the LLNL-CAMS facility (Davis *et al.*, 1990) and normalized the measurements to the ICN (ICN Biomedical, Inc.)  $^{10}\text{Be}$  and the NBS (National Bureau of Standards, presently the National Institute of Standards and Technology, NIST)  $^{26}\text{Al}$  standards.

Production rates for  $^{10}\text{Be}$  and  $^{26}\text{Al}$  in quartz were based on the sea level and high latitude production rates of 6 and 36.8 atoms  $\text{g}^{-1} \text{a}^{-1}$  respectively (Nishiizumi *et al.*, 1989), and were corrected for latitude and altitude effects (Lal, 1991) as well as for the slope and shielding of the sample (Nishiizumi *et al.*, 1989; Dunne *et al.*, 1999; Masarik and Vanya, in press). Here we use these production rates for consistency with previous reports of erosion rates, despite the growing debate over production rates (e.g. Clark *et al.*, 1995; Nishiizumi *et al.*, 1996; Stone *et al.*, 1998a; Dunai, 2000) and the likely contribution of muons to nuclide concentrations under moderate and high erosion rates (e.g. Brown *et al.*, 1995; Stone *et al.*, 1998b; Granger and Smith, in press).

The apparent rates of erosion or soil production were calculated using Equation 14 from both  $^{10}\text{Be}$  and  $^{26}\text{Al}$  concentrations, where applicable, assuming that the initial nuclide concentration was zero (Table I) (Heimsath *et al.*, 1997, 1999; Small *et al.*, 1999) and that the observed local soil depth has been relatively constant over the exposure history of the samples. Observations of the active processes on the landscape suggest, however, that local soil depth is likely to have varied and we discuss the implications of this variation below.

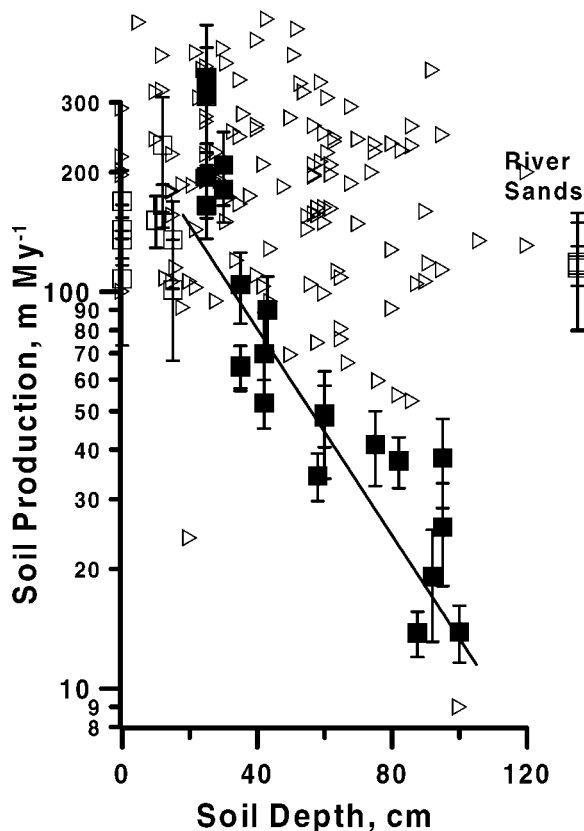


Figure 7. The curvature data from the divergent ( $-\nabla^2 z > 0$ ) areas of Figure 6 converted to soil production rates by Equation 4 using an independently derived diffusivity of  $50 \text{ cm}^2 \text{ a}^{-1}$  (Reneau and Dietrich, 1991) and an observed soil to bedrock bulk density ratio of 0.5, and plotted with the nuclide-determined soil production rates shown on Figure 5

#### THE APPARENT SOIL PRODUCTION FUNCTION

Results from 27 samples ( $^{10}\text{Be}$  and  $^{26}\text{Al}$ ) and eight duplicates ( $^{26}\text{Al}$  only) are reported here to define an apparent soil production function, hard rock erosion rate, and average erosion rate for the field area (Table I). Locations for the nuclide samples from the surveyed area are indicated by the open squares on Figure 4a. Field observations suggested that the bedrock under 15 cm or less soil appeared systematically less weathered than the bedrock under deeper soils, which agreed with the division proposed by Anderson (1995). Soil production rates determined from these samples (open squares on Figure 5) are therefore regarded as hard rock erosion rates and are differentiated from the deeper samples (closed squares on Figure 5). A well-defined, inverse exponential curve fits through the 19 samples and four duplicates taken from under more than 15 cm of soil, which were all from fractured and weathered bedrock. The apparent soil production function is thus defined as the function determined by these samples:

$$\varepsilon(H) = (268 \pm 25)e^{-(0.03 \pm 0.02) \cdot H} \quad (15)$$

where soil production is in  $\text{m Ma}^{-1}$  and the normal soil depth,  $H$ , is in cm. Hard rock erosion rates (three samples and one duplicate) and soil production rates (three samples and two duplicates) from less than 15 cm depth average  $160 \text{ m Ma}^{-1}$ . An alternative soil production function could therefore be a complex polynomial

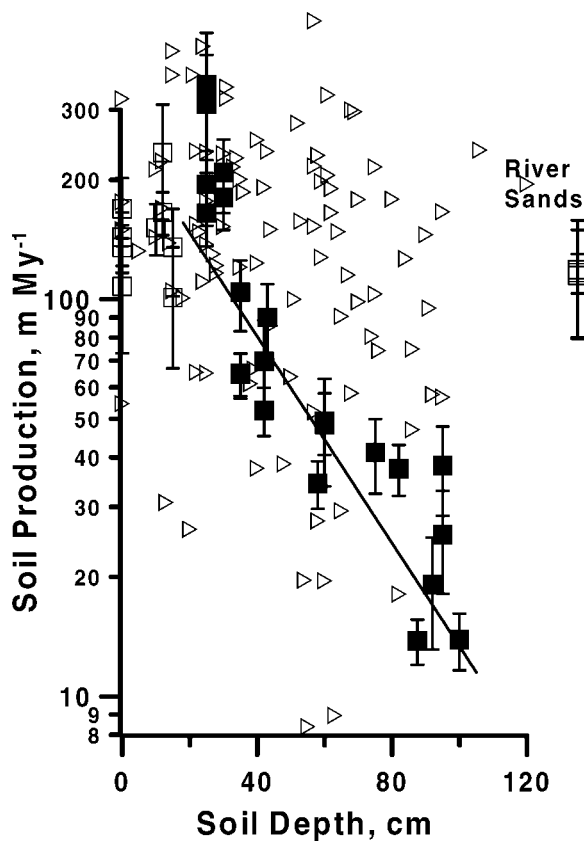


Figure 8. Local erosion rates calculated using Equation 8, which is the solution to Equation 3 using Roering *et al.*'s (1999) non-linear sediment transport model, Equation 7, plotted against observed normal soil depths across both surveyed areas shown in Figure 4a and b. These local erosion rates are plotted with the soil production rates shown on Figure 5 for comparison with Figure 7

one, or 'humped' (*cf* Carson and Kirkby, 1972, pp. 104–106; Cox, 1980) with a maximum soil production rate of  $350 \text{ m Ma}^{-1}$  under 25 cm of soil and a drop to  $160 \text{ m Ma}^{-1}$  as the zero depth intercept. There was, however, little basis for such a function, as the morphologic signature (*i.e.* extensive bedrock outcropping and few areas of shallow soils) of the unstable behaviour suggested by Carson and Kirkby (1972) and modelled by Dietrich *et al.* (1995) was not observed.

The stream sediment samples (two samples and one duplicate) plotted to the right of the soil depth axis (Figure 5) yielded a catchment-averaged erosion rate of  $117 \text{ m Ma}^{-1}$  (Table I). This rate reflects a much larger drainage area than the catchment draining the study area, and is likely to represent a well-mixed average for the region (*e.g.* Bierman and Steig, 1996; Granger *et al.*, 1996).

### MORPHOMETRIC RESULTS

Curvature calculated for each of the 150 soil depth measurements is plotted against the observed slope-normal depth in Figure 6. The filled circles on Figure 4a and b show pit locations and data from the two survey areas are distinguished by different symbols in Figure 6. Curvature shows no relationship with soil thickness for both of the surveyed sites, and while the Headwall region data are slightly more divergent, the data together show considerable scatter. Sample sites were chosen to stay on the divergent ridges (Figure 4a and b), but some sample points show local convergence. The nuclide sample locations are all from divergent

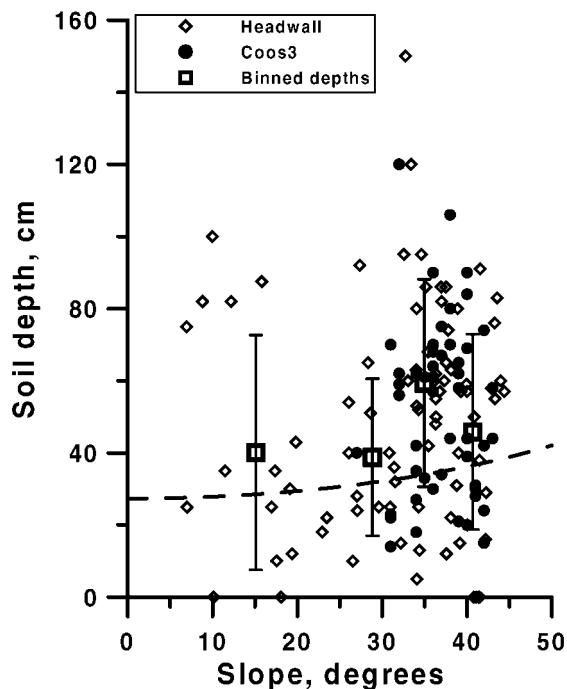


Figure 9. Soil depth plotted against topographic slope from both surveyed areas shown in Figure 4a and b. The symbols are the same as on Figure 6 and the dashed line is the relationship expected if equilibrium lowering conditions applied to the landscape as expressed by Equation 11 in the text. Open squares show binned and averaged values for soil depth and slope with the error bars showing the  $1\sigma$  standard deviation

ridges, but the curvature–depth relationship for those points shows the same scatter as the data shown together in Figure 6. The scatter in these data is clearly indicative of the stochastic soil production and transport processes active at the site and is nearly identical to results reported by Schmidt (1999) for the same field site.

Previous research by Reneau and Dietrich (1991) determined the diffusivity,  $K$ , to be  $50 \text{ cm}^2 \text{ a}^{-1}$  for a field area similar to this site. Roering *et al.* (1999) and Schmidt (1999) report similar values. We solved Equation 4 by multiplying the curvature values plotted on Figure 6 by this diffusivity, the ratio of soil to rock bulk densities (0.5) and the cosine of the local slope at each point to compare these data with the apparent slope-normal soil production rates (Figure 7). There is good agreement between the magnitude of the rates determined by the two independent methods, even if the morphometric method yields no distinct relationship.

Figure 8 shows similar agreement between the soil production rates from nuclide analyses and the magnitude of local erosion rates by using Equation 8, which is the solution of Equation 3 using the non-linear sediment transport model of Roering *et al.* (1999). While Roering *et al.* (1999) may have calibrated their model assuming that all points are lowering at the same rate, the agreement with the nuclide-determined rates shown here adds further support to their model. Both Figures 7 and 8 show considerable scatter across the full range of apparent soil production rates and depths, but the agreement in magnitude of the rates from all methods is encouraging. Roering *et al.* (1999) report that 70 per cent of the landscape evaluated with a non-linear transport model has a modelled erosion rate between  $50$  and  $150 \text{ m Ma}^{-1}$ , which is in good agreement with the results we report here irrespective of the transport model used.

To evaluate the potential for equilibrium conditions we plot soil depth against local slope and use Equation 11 to plot the expected equilibrium relationship between soil depth and slope (Figure 9). Equation 15

determines an  $\alpha$  of 0.03, an  $\varepsilon_0$  of 268 m Ma<sup>-1</sup>, and the catchment-averaged erosion rate of 117 m Ma<sup>-1</sup> from nuclide concentrations in stream sediments is used here as the potential equilibrium lowering rate,  $C_0$ , of the landscape, which agrees well with the average lowering rate of 100 m Ma<sup>-1</sup> by Reneau and Dietrich (1991). The observed depth–slope relationship neither supports nor rejects the equilibrium relationship because of the scatter in the data, but because  $\alpha$ ,  $P_0$  and  $C_0$  were determined independently, the match in values is as important as the comparisons on Figures 7 and 8 for suggesting the comparability of the field methods. Binning the data at different intervals of slope supports more closely the proposed equilibrium relationship (open squares on Figure 9).

## DISCUSSION

Soil production and transport processes at the Coos Bay field site are dominated by the mechanical disruption caused by burrowing animals and root penetration by Douglas fir trees. The stochastic nature of these large-scale processes (compared to, for example, invertebrate soil production and root penetration by understorey vegetation) led to large variations in local soil thickness on the divergent noses. There were no observed relationships between curvature (as a proxy for soil production using a linear transport model) and soil depth as observed by Heimsath *et al.* (1997, 2000), or between erosion calculated from a non-linear transport model (e.g. Roering *et al.*, 1999) and depth. Despite these variations in processes, however, there was a well-defined relationship between soil production rates from the radionuclide analyses and soil depth that we term here the apparent soil production function (Figure 5, Equation 15) because of the assumption of steady-state local soil depth used to determine the function. This discrepancy between the two methods highlights an interesting paradox that is not immediately resolvable.

The first implication of the stochastic conditions observed here on the cosmogenic nuclide method is that the soil depths observed in the field might not represent the long-term average soil under which the observed nuclide concentrations accumulated. The second implication is that the nuclide concentrations measured from the underlying bedrock might not represent the effect of the long-term average soil production rate at any given location. Both implications would suggest that results from the nuclide analyses would show considerably more scatter than observed here. Instead, if the observed depths do represent a local average depth, then the apparent relationship suggests that there is a strong tendency for soil production rates to decline with depth. The well-defined inverse exponential apparent soil production function is similar to the findings reported for northern California (Heimsath *et al.*, 1997, 1999) and for southeastern Australia (Heimsath *et al.*, 2000), from field areas without large-scale disturbances of the soil and soil–bedrock interface.

The only possibility of an artifactual relationship lies in the factor applied to correct the nuclide production rates for the slope and the shielding of the overlying soil thickness. If, for example, the central tendency for the weathered bedrock is to be eroding at some equilibrium rate (discussed below) irrespective of the overlying soil thickness, then nuclide concentrations measured in all samples would show some scatter around a mean value. Interpreting the nuclide concentrations using Equation 14 requires accounting for the shielding of the soil mantle and would lower the nuclide production rates for increasing soil depths. Lowering the nuclide production rates would lower the inferred soil production rates by Equation 14, thus potentially introducing an artifact due to the observed depth. An artifactual relationship would have a slope of about  $-0.008$  ( $=\rho_s/\Lambda$ , assuming an average moist soil density of 1.4 g cm<sup>-3</sup>), which is four times less steep than the slope of Equation 15, suggesting that the apparent soil production function reported here is not an artifact.

The potential effects of the non-steady-state erosion on the observed nuclide concentrations have been modelled numerically in several studies (Lal, 1991; Bierman and Steig, 1996; Small *et al.*, 1997). Each of these models integrated their equivalent of Equation 12 under episodic (Lal, 1991; Small *et al.*, 1997) and a step-function of (Bierman and Steig, 1996) erosion rates. While Lal (1991) modelled a very specific scenario where a rock erodes at a constant rate before and after a 50 cm thick ‘chip’ is removed instantaneously, Small *et al.* (1997) present a model applicable here. Their finite-difference model evaluates the potential error of determining erosion rates from nuclide concentrations that have accumulated under episodic erosion events

that remove different amounts of rock at different time intervals. In all modelled cases they calculate the magnitude of error incurred by using the non-steady-state nuclide concentrations to infer steady-state erosion rates. By their modelled conditions the steady-state soil production rates that we report here would have between a 20 and 30 per cent error if the stochastic soil production processes remove 50 cm of bedrock at a time. The error would be larger (up to 200 per cent) if we sampled relatively recently after an episodic disturbance.

None of these models, however, accounted for the potential variation in a soil mantle shielding the sample. Heimsath and Barnes (unpublished data) have developed a similar numerical model that builds on the results of Bierman and Steig (1996) and Small *et al.* (1997) to add an analysis of the uncertainty caused by a variable soil mantle such as we faced here. Their results suggest that the episodically varying soil mantle could introduce an additional 10–20 per cent error into the inferred soil production rates, with the uncertainty increasing if a large event recently preceded the time of sampling. The conclusions reached, however, agree with both Bierman and Steig (1996) and Small *et al.* (1997), as well as with previous discussions by Lal (1991): the *in situ*-produced radionuclide method depends explicitly on the samples having a steady-state erosion history. Deviations from such a condition could lead to incorrect modelling of the exposure history and therefore incorrect interpretations of the radionuclide concentrations. In the absence of accurate knowledge of the exposure histories of samples, the best that can be done is to sample from locations that appear free from large-scale perturbations as we have done here. This remains an important point to make as further geomorphic applications are being tackled with radionuclide measurements.

While our observations and those of Schimdt (1999) show very clearly that stochastic and large-scale processes are occurring across the field area, we remain optimistic that our careful selection of nuclide sampling sites may have avoided the local effects of recent stochastic processes. Conversely, our sampling strategy for measuring soil depth for the morphometric analyses was to measure depths in a rough grid across the divergent parts of the landscape, seeking only to avoid any obvious disturbances on the landsurface, which therefore captured the uncorrelated variation of soil depth across the landscape. The scatter in our morphometric data is very similar to that observed by Schmidt (1999), although his estimates of colluvial production rates from morphometric analyses shows a weak inverse relationship.

Ahnert (1987) presents a compelling argument for how spatial variation of rock resistance to soil production can lead to variable soil depths on a one-dimensional landscape that tends toward equilibrium. His model posits a lower maximum soil production rate,  $\epsilon_0$  in Equation 5, for more resistant rock and evolves to a state where the exposed harder rock is lowering at the same rate as the soil-mantled, more easily erodible rock. Our nuclide results (Figure 5) suggest that such a scenario might help explain some of the depth variation, but the large variation in soil production rates for the more easily erodible rock suggests a more complicated interaction between hillslope processes and form. An important step toward resolving the paradox between morphometric observations and the apparent soil production function would be to quantify the role of bedrock strength and its resistance to mechanical weathering. Similarly, measurements to determine how the depth of the saprolite layer varies (e.g. Anderson, 1995), combined with correlating rock strength to soil production rates, would help link chemical weathering to soil production processes.

Many factors, from climate to tectonics, influence the evolution of a landscape. At a hillslope scale, the sediment production and transport processes directly influence the way a landscape changes. Most landscape evolution models simulate hillslope erosion as a steady-state process using a linear diffusion model, but Roering *et al.* (1999) present evidence that a non-linear transport model is appropriate for this field area. Morphometric analyses reported here cannot distinguish between the two models, but we specifically avoided the planar and steep slopes to remain out of the region where the non-linear model may predict sediment flux more closely than the linear model, as suggested by Roering *et al.* (1999). Irrespective of the transport law most applicable to the landscape – and it appears likely that a single transport law cannot adequately capture the processes (Heimsath *et al.*, 2000; Braun, Heimsath and Chappell, 2001) – the evidence from Oregon is of a landscape shaped by the continuous interaction between stochastic hillslope processes and the driving forces of stream incision and tectonic uplift. Reneau and Dietrich (1991) suggest that this interaction approaches equilibrium tendencies at the landscape scale. Here, the apparent soil production function coupled

with the observed variation in soil depth supports a state of local hillslope disequilibrium as discussed in Heimsath *et al.* (1997, 1999). The lack of morphometric relationships suggests, however, that the differences in soil production rates may act across the hillslope toward a uniformity of hillslope lowering rates over long time scales.

### CONCLUSIONS

Here we report an apparent soil production function for a well-studied field site in the Oregon Coast Range. The well-defined exponential decline of soil production rates with increasing soil depths is similar to the functions reported elsewhere from field areas under very different climatic, tectonic and lithologic conditions in Marin County, California and southeastern Australia. This agreement suggests that there is a universal tendency for soil production rates to depend on the overlying soil thickness across hilly landscapes. As we have discussed before, and numerous recent models have applied, this relationship provides critical constraints for the processes of landscape evolution. The maximum soil production rate is, for example, the bound between transport-limited (soil-mantled) and weathering-limited (bedrock-dominated) landscapes and thus quantifies the maximum erosion rate under which a landscape can remain soil-mantled. This has important management implications in a landscape such as the Oregon Coast Range, where human land-use might be increasing erosion rates.

Morphometric analyses here did not yield the form of the soil production function, but provided evidence for the stochastic and large-scale nature of the soil production and transport processes. Field observations on the nature of soil production and removal show episodic processes of tree-throw, animal burrowing and shallow landsliding operating across the landscape. These processes lead to highly variable local soil depths over time and measurements of soil depth may only reflect an instantaneous snapshot of the soil depths across the landscape, rather than the long-term, steady-state soil thickness assumed for our nuclide interpretations. Stochastic processes also lead to highly variable erosion rates at the hillslope scale. Despite these variations, we conclude that the apparent soil production function reported here provides a valid and crucial quantification for the Oregon Coast Range landscape.

The study area is a small part of a landscape that is being shaped by a wide variety of processes. The catchment-averaged erosion rates determined by nuclide analyses here agree well with the rates determined by other methods across temporal and spatial scales for the Oregon Coast Range and suggest that there may be a tendency for uniformity of erosion at a large scale as suggested by Reneau and Dietrich (1991). Similarity in landscape form at the catchment scale supports this conclusion, while the highly variable hillslope processes highlight the local variation in erosion rates. While there may be some average erosion rate that applies to similar topography across the Oregon Coast Range, it is clear that local hillslopes are far from conditions of uniform lowering rates. The determination of an apparent soil production function for the region suggests that different parts of the landscape are lowering at rates that differ by over an order of magnitude depending on the thickness of the local soil mantle, and are therefore evolving in a highly dynamic manner.

### ACKNOWLEDGEMENTS

We thank Kabir Heimsath for assisting with the surveys of the Headwall region and Josh Roering for help with Coos3 and with making the laser altimetry data useful for this work. Thanks also to the Weyerhaeuser Corporation for continuing to make the Coos Bay field area accessible for such research. Discussions in the field with Alan Howard, Leonard Sklar, Josh Roering and David Montgomery were very helpful. NSF grant EAR-9527006, Cal Space grant IGPP-LLNL GS96-05 and NASA Global Change and Switzer Environmental Fellowships to Heimsath supported this work. Nuclide measurements were partially performed under the auspices of the US DOE by Lawrence Livermore National Laboratory under contract W-7405-Eng-48, and we thank Don DePaolo for laboratory space. Thanks to Mike Kirkby and an anonymous reviewer for their helpful comments.

## REFERENCES

- Ahnert F. 1987. Approaches to dynamic equilibrium in theoretical simulations of slope development. *Earth Surface Processes and Landforms* **12**: 3–15.
- Anderson RS. 1994. Evolution of the Santa Cruz mountains, California, through tectonic growth and geomorphic decay. *Journal of Geophysical Research – Solid Earth* **99**(B10): 20161–20179.
- Anderson RS, Humphrey NF. 1989. Interaction of weathering and transport processes in the evolution of arid landscapes. In *Quantitative Dynamic Stratigraphy*, Cross T (ed), Prentice Hall: Englewood Cliffs, NJ. 349–361.
- Anderson SP. 1995. *Flow paths, solute sources, weathering, and denudation rates; the chemical geomorphology of a small catchment*. PhD thesis, University of California, Berkeley.
- Beier P. 1989. Use of habitat by mountain beaver in the Sierra Nevada. *Journal of Wildlife Management* **53**(3): 649–654.
- Benda L, Dunne T. 1997. Stochastic forcing of sediment supply to channel networks from landsliding and debris flow. *Water Resources Research* **33**: 2849–2863.
- Beschta RL. 1978. Long-term patterns of sediment production following road construction and logging in the Oregon Coast Range. *Water Resources Research* **14**: 1011–1016.
- Bierman P, Steig EJ. 1996. Estimating rates of denudation using cosmogenic isotope abundances in sediment. *Earth Surface Processes and Landforms* **21**: 125–139.
- Bierman PR. 1994. Using in situ produced cosmogenic isotopes to estimate rates of landscape evolution; a review from the geomorphic perspective. *Journal of Geophysical Research, B, Solid Earth and Planets* **99**(7): 13 885–13 896.
- Bleich VC, Racine D. 1991. Mountain beaver (*Aplodontia rufa*) from Inyo County, California. *California Fish and Game* **77**(3): 153–155.
- Brown ET, Bowles DL, Colin F, Raisbeck GM et al. 1995. Evidence for muon-induced production of  $^{10}\text{Be}$  in near-surface rocks from the Congo. *Geophysical Research Letters* **22**(6): 703–706.
- Brown GW, Krygier JT. 1971. Clear-cut logging and sediment production in the Oregon Coast Range. *Water Resources Research* **7**(5): 1189–1198.
- Brown J, Heimsath AM, Chappell J. 2001. Sediment transport mechanisms on soil-mantled hillslopes. *Geology* (in press).
- Carson MA, Kirkby MJ. 1972. *Hillslope Form and Process*. Cambridge University Press: New York.
- Cerling TE, Craig H. 1994. Geomorphology and in-situ cosmogenic isotopes. *Annual Review of Earth and Planetary Sciences* **22**: 273–317.
- Clark DH, Bierman PR, Larsen P. 1995. Improving in situ cosmogenic chronometers. *Quaternary Research* **44**: 367–377.
- Cox NJ. 1980. On the relationship between bedrock lowering and regolith thickness. *Earth Surface Processes and Landforms* **5**: 271–274.
- Cressie NAC. 1991. *Statistics for Spatial Data*. John Wiley and Sons: New York.
- Culling WEH. 1960. Analytical theory of erosion. *The Journal of Geology* **68**: 336–344.
- Culling WEH. 1963. Soil creep and the development of hillside slopes. *The Journal of Geology* **71**(2): 127–161.
- Davis JC, Proctor ID, Southam JR et al. 1990. LLNL/UC AMS facility and research program. *Nuclear Instruments Methods in Physics Research, Section B* **52**: 269–272.
- Davis WM. 1892. The convex profile of badland divides. *Science* **20**: 245.
- Denny CS, Goodlett JC. 1957. Microrelief resulting from fallen trees. *USGS Professional Paper* **288**: 59–68.
- Dietrich WE, Dunne T. 1978. Sediment budget for a small catchment in mountainous terrain. *Zeitschrift für Geomorphologie Supplementband* **29**: 191–206.
- Dietrich WE, Dunne T, Humphrey NF, Reid LM. 1982. Construction of sediment budgets for drainage basins. In *Sediment Budgets and Routing in Forested Drainage Basins*, Swanson FJ, Janda RJ, Dunne T, Swanson DN (eds). USDA Forest Service Technical Report PNW-141: 5–23.
- Dietrich WE, Wilson CJ, Reneau SL. 1986. Hollows, colluvium, and landslides in soil-mantled landscapes. In *Hillslope Processes*, Abrahams AD (ed.). Binghamton Symposia in Geomorphology, International Series. Allen and Unwin: 361–388.
- Dietrich WE, Reiss R, Hsu M-L, Montgomery DR. 1995. A process-based model for colluvial soil depth and shallow landsliding using digital elevation data. *Hydrological Processes* **9**: 383–400.
- Dunai TJ. 2000. Scaling factors for production rates of in situ produced cosmogenic nuclides: a critical reevaluation. *Earth and Planetary Science Letters* **176**: 157–169.
- Dunne J, Elmore D, Muzikar P. 1999. Scaling factors for the rates of production of cosmogenic nuclides for geometric shielding and attenuation at depth on sloped surfaces. *Geomorphology* **27**(1–2): 3–11.
- Fitts KM. 1996. Observations on use of two non-native plants by the Point Arena mountain beaver. *California Fish and Game* **82**(1): 59–60.
- Gilbert GK. 1877. *Report on the Geology of the Henry Mountains (Utah)*. United States Geological Survey: Washington, D.C.
- Gilbert GK. 1909. The convexity of hilltops. *Journal of Geology* **17**(4): 344–350.
- Granger DE, Smith AL. (in press). Dating buried sediments using radioactive decay and muogenic production of  $^{26}\text{Al}$  and  $^{10}\text{Be}$ . *Nuclear Instrumentation and Methods in Physics Research B*.
- Granger DE, Kirchner JW, Finkel R. 1996. Spatially averaged long-term erosion rates measured from in situ-produced cosmogenic nuclides in alluvial sediment. *Journal of Geology* **104**(3): 249–257.
- Haagen JT. 1989. *Soil Survey of Coos County, Oregon*. USDA, Soil Conservation Service: Roseburg, Oregon.
- Hack JT. 1960. The interpretation of erosional topography in humid temperate regions. *American Journal of Science* **258A**: 80–97.
- Heimsath AM, Dietrich WE, Nishiizumi K, Finkel RC. 1997. The soil production function and landscape equilibrium. *Nature* **388**: 358–361.
- Heimsath AM, Dietrich WE, Nishiizumi K, Finkel RC. 1999. Cosmogenic nuclides, topography, and the spatial variation of soil depth. *Geomorphology* **27**(1–2): 151–172.

- Heimsath AM, Chappell J, Dietrich WE, Nishiizumi K, Finkel RC. 2000. Soil production on a retreating escarpment in southeastern Australia. *Geology* **28**: 787–790.
- Heller PL, Peterman ZE, O'Neil JR, Shafiqullah M. 1985. Isotopic provenance of sandstones from the Eocene Tyee Formation, Oregon Coast Range. *Geological Society of America Bulletin* **96**: 770–780.
- Hirano M. 1968. A mathematical model of slope development – an approach to the analytical theory of erosional topography. *Journal of Geosciences* **11**(2): 13–52.
- Hole FD. 1981. Effects of animals on soil. *Geoderma* **25**: 75–112.
- Howard AD. 1994. A detachment-limited model of drainage basin evolution. *Water Resources Research* **30**(7): 2261–2285.
- Howard AD. 1997. Badland morphology and evolution: interpretation using a simulation model. *Earth Surface Processes and Landforms* **22**: 211–227.
- Johnson KA, Sitar N. 1990. Hydrologic conditions leading to debris-flow initiation. *Canadian Geotechnical Journal* **27**: 789–801.
- Kelsey HM. 1990. Late Quaternary deformation of marine terraces on the Cascadia subduction zone near Cape Blanco. *Tectonics* **9**: 983–1014.
- Kelsey HM, Bockheim JG. 1994. Coastal landscape evolution as a function of eustasy and surface uplift rates, Cascadia margin, southern Oregon. *Geological Society of America Bulletin* **106**: 840–854.
- Kelsey HM, Engebretson DC, Mitchell CE, Ticknor RL. 1994. Topographic form of the Coast Ranges of the Cascadia margin in relation to coastal uplift rates and plate subduction. *Journal of Geophysical Research* **99**: 12,245–12,255.
- Kirkby MJ. 1967. Measurement and theory of soil creep. *The Journal of Geology* **75**(4): 359–378.
- Kirkby MJ. 1971. Hillslope process–response models based on the continuity equation. *Institute of British Geographers Special Publication* **3**: 15–30.
- Kirkby MJ. 1985. A model for the evolution of regolith-mantled slopes. In *Models in Geomorphology*, Woldenburg MJ (ed.). Allen and Unwin: Winchester, MA; 213–237.
- Kohl CP, Nishiizumi K. 1992. Chemical isolation of quartz for measurement of in-situ produced cosmogenic nuclides. *Geochimica et Cosmochimica Acta* **56**: 3583–3587.
- Lal D. 1988. In situ-produced cosmogenic isotopes in terrestrial rocks. *Annual Review of Earth and Planetary Science* **16**: 355–388.
- Lal D. 1991. Cosmic ray labeling of erosion surfaces: in situ nuclide production rates and erosion models. *Earth and Planetary Science Letters* **104**: 424–439.
- Lal D, Arnold JR. 1985. Tracing quartz through the environment. *Proceedings of the Indian Academy of Science (Earth and Planetary Science)* **94**(1): 1–5.
- Lovell JPB. 1969. Tyee Formation: undeformed turbidites and their lateral equivalents: mineralogy and paleogeography. *Geological Society of America Bulletin* **80**: 9–22.
- Lutz HJ. 1940. Disturbance of forest soil resulting from the uprooting of trees. *Yale University Forestry Bulletin* **45**: 1–37.
- Lutz HJ. 1960. Movement of rocks by uprooting of forest trees. *American Journal of Science* **258**: 752–756.
- Lutz HJ, Griswold FS. 1939. The influence of tree roots on soil morphology. *American Journal of Science* **258**: 389–400.
- Lyford WH, MacLean DW. 1966. *Mound and pit microrelief in relation to soil disturbance and tree distribution in New Brunswick, Canada*. Harvard Forest, Harvard University: Petersham, MA.
- Masarik J, Vanya S. 2000. Numerical simulation of in-situ production of cosmogenic nuclides: effects of irradiation geometry. *Nuclear Instrumentation and Methods in Physics Research B*.
- Matsuoka N. 1990. The rate of bedrock weathering by frost action: field measurements and a predictive model. *Earth Surface Processes and Landforms* **15**: 73–90.
- McKean JA, Dietrich WE, Finkel RC, Southon JR, Caffee MW. 1993. Quantification of soil production and downslope creep rates from cosmogenic  $^{10}\text{Be}$  accumulations on a hillslope profile. *Geology* **21**(4): 343–346.
- Mitchell P. 1988. The influences of vegetation, animals and micro-organisms on soil processes. In *Biogeomorphology*, Viles HA (ed.). Basil Blackwell: New York; 43–82.
- Montgomery DR, Dietrich WE, Torres R, Anderson SP, Heffner JT, Logue K. 1997. Hydrologic response of a steep, unchanneled valley to natural and applied rainfall. *Water Resources Research* **33**(1): 91–109.
- Nishiizumi K, Lal D, Klein J, Middleton R, Arnold JR. 1986. Production of  $^{10}\text{Be}$  and  $^{26}\text{Al}$  by cosmic rays in terrestrial quartz in situ and implications for erosion rates. *Nature* **319**(6049): 134–136.
- Nishiizumi K, Winterer K, Kohl CP, Klein J, Middleton R, Lal D, Arnold JR. 1989. Cosmic ray production rates of  $^{10}\text{Be}$  and  $^{26}\text{Al}$  in quartz from glacially polished rocks. *Journal of Geophysical Research* **94**(B12): 17 907–17 915.
- Nishiizumi K, Kohl CP, Arnold JR, Klein J, Fink D, Middleton R. 1991. Cosmic ray produced  $^{10}\text{Be}$  and  $^{26}\text{Al}$  in Antarctic rocks; exposure and erosion history. *Earth and Planetary Science Letters* **104**(2–4): 440–454.
- Nishiizumi K, Kohl CP, Arnold JR, Dorm R, Klein J, Fink D, Middleton R, Lal D. 1993. Role of in situ cosmogenic nuclides  $^{10}\text{Be}$  and  $^{26}\text{Al}$  in the study of diverse geomorphic processes. *Earth Surface Processes and Landforms* **18**: 407–425.
- Nishiizumi K, Finkel RC, Klein J, Kohl CP. 1996. Cosmogenic production of  $^7\text{Be}$  and  $^{10}\text{Be}$  in water targets. *Journal of Geophysical Research* **101**(B10): 22 225–22 232.
- Norman SA, Schaeztl RJ, Small TW. 1995. Effects of slope angle on mass movements by tree uprooting. *Geomorphology* **14**: 19–27.
- Orr EL, Orr WN, Baldwin EM. 1992. *Geology of Oregon*. Kendall/Hunt: Dubuque.
- Paton TR, Humphries GS, Mitchell PB. 1995. *Soils: a new global view*. UCL Press: London.
- Persson SF. 1995. Late Quaternary stream incision and uplift in the forearc of the Cascadia subduction zone, western Oregon. *Journal of Geophysical Research* **100**(B10): 20 193–20 210.
- Pierson TC. 1977. *Factors controlling debris-flow initiation on forested hillslopes in the Oregon Coast Range*. PhD Thesis, University of Washington, Seattle.
- Reneau SL, Dietrich WE. 1990. Depositional history of hollows on steep hillslopes, coastal Oregon and Washington. *National Geographic Research* **6**(2): 220–230.

- Reneau SL, Dietrich WE. 1991. Erosion rates in the southern Oregon coast range: evidence for an equilibrium between hillslope erosion and sediment yield. *Earth Surface Processes and Landforms* **16**(4): 307–322.
- Roering JJ, Kirchner JW, Dietrich WE. 1999. Evidence for non-linear, diffusive sediment transport on hillslopes and implications for landscape morphology. *Water Resources Research* **35**(3): 853–870.
- Rosenbloom NA, Anderson RS. 1994. Hillslope and channel evolution in a marine terraced landscape, Santa Cruz, California. *Journal of Geophysical Research* **99**(B7): 14 013–14 029.
- Schaetzl RJ, Follmer LR. 1990. Longevity of treethrow microtopography: implications for mass wasting. *Geomorphology* **3**: 113–123.
- Schmidt K. 1999. *Root strength, colluvial soil depth, and colluvial transport on landslide-prone hillslopes* PhD Thesis, University of Washington, Seattle.
- Schumm SA. 1967. Rates of surficial rock creep on hillslopes in Western Colorado. *Science* **155**: 560–562.
- Small EE, Anderson RS, Repka JL, Finkel R. 1997. Erosion rates of alpine bedrock summit surfaces deduced from in situ  $^{10}\text{Be}$  and  $^{26}\text{Al}$ . *Earth and Planetary Science Letters* **150**(3–4): 413–425.
- Small EE, Anderson RS, Hancock GS, Finkel RC. 1999. Estimates of regolith production from  $^{10}\text{Be}$  and  $^{26}\text{Al}$ : Evidence for steady state alpine hillslopes. *Geomorphology* **27**(1–2): 131–150.
- Snively PD, Wagner HC, MacLeod NS. 1964. Rhythmic-bedded eugeosynclinal deposits of the Tye Formation, Oregon Coast Range. *Kansas Geological Survey Bulletin* **169**: 461–480.
- Stephens EP. 1956. The uprooting of trees: a forest process. *Soil Science Society Proceedings* 113–116.
- Stone JO, Ballantyne CK, Fifield LK. 1998a. Exposure dating and validation of periglacial weathering limits, northwest Scotland. *Geology* **26**(7): 587–590.
- Stone JO, Evans JM, Fifield LK, Allan GL, Cresswell RG. 1998b. Cosmogenic chlorine-36 production in calcite by muons. *Geochimica et Cosmochimica Acta* **62**(3): 433–454.
- West DO, McCrumb DR. 1988. Coastline uplift in Oregon and Washington and the nature of Cascadia subduction-zone tectonics. *Geology* **16**: 169–172.
- Yee CS, Harr RD. 1977. Influence of soil aggregation on slope stability in the Oregon Coast Ranges. *Environmental Geology* **1**: 367–377.